

FIELD OBSERVATIONS OF SUSPENDED SEDIMENT CONCENTRATION, TURBULENCE, AND BEDFORMS

Drude F. Christensen¹ and Troels Aagaard¹

Abstract

Three different examples of intra-wave variations in suspended sediment concentration (SSC) were examined in relation to turbulence level and bed morphology. Measurements were collected on the seaward slope of an intertidal bar during both breaking and non-breaking wave conditions. During non-breaking conditions with presence of vortex ripples the sediment suspension was dominated by vortex shedding. When suborbital ripples were present, a simple proportionality existed between SSC and the wave orbital velocity. Thus, the largest suspended sediment concentrations existed at the time of maximum velocities and for velocity skewed waves this resulted in a net onshore wave-induced sediment transport. During breaking wave conditions coherent breaker eddies appeared on the onshore wave phase causing high SSCs and a net onshore wave-induced sediment transport.

Key words: suspended sediment concentration, turbulence, bed morphology, cross-shore wave-induced sediment transport

1. Introduction

The suspended sediment concentration under irregular waves varies in magnitude and timing within the wave cycle and intra-wave variations are of great importance for the net wave-induced sediment transport direction due to the orbital motion of the waves. During low-moderate energy conditions the non-steady oscillatory wave motion dominates the sediment transport which tends to cause net onshore sediment transport. Presently available transport models are, however, often incapable of simulating this onshore transport with confidence (Mariño-Tapia et al., 2007). Many numerical transport models are based on the energetics approach which relates sediment transport to the near-bed wave orbital motions (Bagnold, 1966) and hence, velocity skewness is the principal cause for an onshore sediment transport. The limited ability of the energetics based models to predict onshore sediment transport, nevertheless, indicates that velocity skewness alone may be insufficient to explain the observed transport.

An important shortcoming of the models is the assumption of proportionality between time dependent orbital velocity and suspended sediment concentration. For instance, presence of bedforms may disrupt the proportionality, as for example vortex ripples may cause sediment suspension events and peak concentrations at the time of flow reversal (O'Hara Murray et al., 2011).

Several mechanisms, presently omitted in the transport models, have been suggested to contribute to an onshore sediment transport by causing near-bed turbulence, and thereby sediment stirring, on the onshore wave phase. Acceleration skewness is hypothesised to cause an onshore sediment transport due to an emerging onshore pressure gradient and a thin wave boundary layer enhancing shear stress on the onshore wave phase (Nielsen, 2006). Field measurements have shown a close correlation between acceleration skewness and sandbar crest location (Elgar et al., 2001). This indicates that acceleration skewness could be of importance for observed onshore sandbar migration. Acceleration skewness is, however, often correlated to surface-generated turbulence, and it is therefore possible that it is the surface-generated turbulence which is critical to the sediment suspension beneath the wave crest (Puleo et al., 2003; Aagaard and Hughes, 2010). Surface-generated turbulence can be large all the way to the bed (Scott et al., 2005; Ruessink, 2010; Grasso et al., 2012) and in particular plunging breakers tend to be of significant

¹Department of Geosciences and Natural Resource Management, University of Copenhagen, Denmark. dc@ign.ku.dk; taa@ign.ku.dk

importance for sediment suspension (Aagaard and Hughes, 2010; Yoon and Cox, 2012). Under spilling breakers turbulence can stretch towards the bed as obliquely descending eddies behind the wave crest but turbulent kinetic energy is typically smaller compared to plunging breakers (Nadaoka et al., 1989; Scott et al., 2009).

Examinations of the relation between turbulence, suspended sediment concentration and bedform dimensions in the field are limited in number, and knowledge of the timing and magnitude of surface- and bed-generated turbulence within the wave cycles, and the way that it affects sediment suspension, is insufficient. In this paper, three examples of intra-wave variations in suspended sediment concentration are presented. The examples represent different wave and bedform conditions (breaking/non-breaking, megaripples/wave ripples). The applied field measurements were obtained by Larsen et al. (2015) on a beach at Skallingen on the west coast of Jutland, Denmark. The aim of the paper is to relate the observed intra-wave variations in suspended sediment concentration to turbulence level and bedform type.

2. Methods

2.1 Field site and experimental conditions

The beach at the barrier spit Skallingen is located on the Danish North Sea coast with a shore-normal orientation towards the south-west. The barrier is exposed to wind waves with a mean annual significant height of 1.1 m and a mean wave period of 4-5 sec. The beach is dissipative with a gently sloping upper shoreface and two subtidal bars. Moreover, one or more intertidal bars exist in the intertidal zone. The tide is semidiurnal with a mean tidal range of 1.5 m and a spring tidal range of 1.8 m (Aagaard and Hughes, 2006).

Data was collected in September-October 2012, in the intertidal zone near mean water level. The instruments were positioned at the seaward slope of the inner intertidal bar (Fig. 1) where the mean sediment grain size was 240 μm . During the field campaign the offshore significant wave height (H_s) ranged between 0.4-1.8 m and had a peak wave period between 5 and 8 s (Fig. 2). The inshore H_s (at the instrument) was up to 0.7 m. Breaking waves were predominately spilling (Larsen et al., 2015). In this paper the focus is on September 28, September 29, and October 4, with respectively shoaling wave conditions on the 28th and the 4th (run 42 and 337), and spilling breakers on the 29th (run 98).

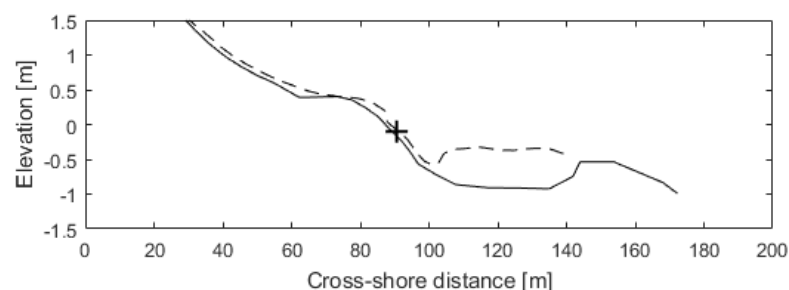


Figure 1. The cross-shore beach profile measured at low tide on September 29 (solid line) and October 6 (dashed line). The distance is related to the top of the aeolian dune ($x = 0$). The position of the tripod is marked by the plus-sign

2.2 Instrumentation and initial data processing

The instrument station (Fig. 3) consisted of a stainless steel tripod to which the following instruments were mounted: a 5 MHz SonTek Acoustic Doppler Velocimeter (ADV) integrated with a piezoresistive pressure sensor, two Optical Backscatters (OBS-3) and an Imagenex 881A pencil-beam sonar combined with an azimuth drive. The ADV and upper OBS were initially placed about 10 cm above the bed, while the lower OBS was located at nominally 5 cm above the bed. The pencil-beam sonar was mounted on an arm, on the tripod, pointing seaward and to the south in order to minimize the risk that scour holes around the legs of the tripod would affect the measurements. The initial installation-height of the sonar was 55 cm above the

bed.

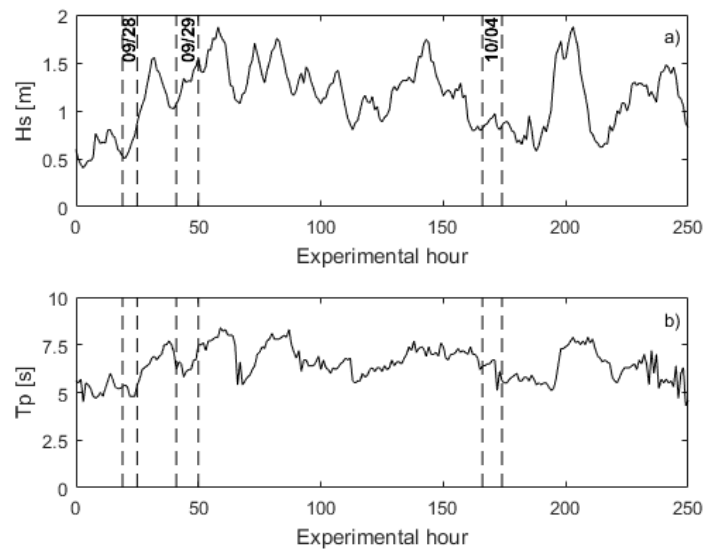


Figure 2. Significant wave height (a) and peak wave period (b) seaward of the surf zone at 6 m water depth off Fanø during the field campaign in 2012. The days of data collection used here are indicated by vertical dashed lines

Measurements of flow velocity, pressure, and suspended sediment concentrations were conducted in periods of 17 minutes every half-hour. The ADV used a sampling frequency of 16 Hz, and it was oriented to measure positive flows to the north, onshore and upward. The estimated flow velocities from the ADV have been rotated in order to minimize small tilt errors of the sensors. Instrument noise in velocity time series recorded by acoustic sensors is very common, especially, in the surf zone due to the presence of air bubbles. Signals with a correlation value lower than an applied threshold of 62 %, have been replaced by a filtered value obtained from a 1 second moving average (Larsen et al., 2015).

A few spikes in the OBS records ($c > c + 10\sigma$), probably due to air bubbles, were replaced with linearly interpolated values. Moreover, saturated values due to instrument burial as well as measurements obtained less than 4 cm above the bed were rejected, since the latter are likely to have been affected by enhanced suspended sediment concentration due to flow disturbance. Consequently, all the measurements obtained by the lower OBS were discarded. In relation to signal calibration, the field offset of the OBS signals were determined to correspond to the 2nd percentile of the measured OBS signals.

The pencil-beam sonar was set to a scan-width of 3 m, and only scans perpendicular to the coastline were obtained. Details on data processing can be found in Larsen et al. (2015).



Figure 3. The tripod with the installed instruments at low tide on September 30, 2012

2.3 Data analysis

A main task of the paper is to isolate the turbulent motions from organized wave motions in the velocity records, and several methods are applicable e.g. ensemble averaging, frequency cut-off, velocity-differencing, and vertical velocity variance (Aagaard and Hughes, 2010). It is, though, a nontrivial task which none of the presently available methods solve to satisfaction. For instance, the ensemble averaging method where phase-averages of the velocity measurements are computed, and the residual is defined as turbulence, is only applicable to regular waves in the laboratory. The frequency cut-off technique, where a change in spectral slope is used to indicate the transition from dominance of orbital wave motion to turbulent motion, is likely to omit large-scale turbulent eddies. In the velocity-differencing method, velocity differences between two adjacent sensors, separated by a distance which is small in relation to the wavelength but large in relation to the turbulent length scale, are defined as turbulence. A weakness of this technique is how to determine the right separation distance compared to the present turbulent length scale, and moreover, if the sensors are placed in the same vertical level, it is required that the waves are unidirectional so that the sensor separation axis is orientated parallel to the wave crests. Finally, in order for vertical velocity variance to represent only turbulent motions, measurements must be conducted very close to the bed, where the orbital wave motion is assumed to be only horizontal (Aagaard and Hughes, 2010).

In this paper the frequency cut-off method has been applied initially as the waves were irregular, measurements were only available from one ADV, and the measuring height (c 10 cm) was too high to assume that the velocity measurements were unaffected by wave orbital motions.

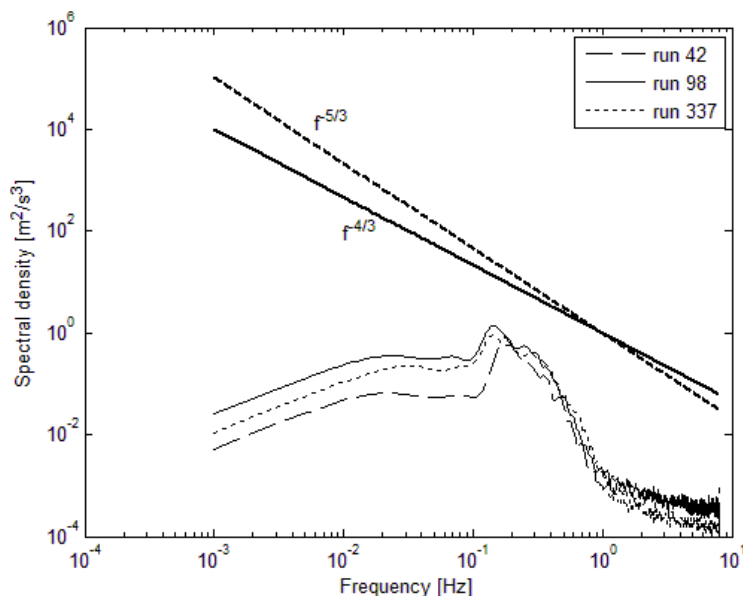


Figure 4. Windowed spectral density plots on logarithmic axes and lines having a slope of respectively $-5/3$ (dashed) and $-4/3$ (solid) indicating turbulent cascade

Fig. 4 illustrates autospectra of cross-shore velocity with an applied 50-point Hanning filter. The spectra have a break in the slope near $f = 1$ Hz. For frequencies above 1 Hz the spectral densities decrease at a rate of about $-4/3$. The spectral slope is thus flatter than expected for the inertial subrange, where the rate of cascade for turbulent energy is assumed to be $-5/3$ (Seuront et al., 2005). However, flatter spectral slopes near the bed have been reported in other studies (e.g. Smyth et al., 2002). Turbulence is therefore assumed to dominate the fluid motions at frequencies greater than 1 Hz.

To test the selected cut-off frequency for the possibility of erroneously omitting large-scale turbulent eddies, co-spectra of cross-shore (u) and vertical velocity (w) is calculated (Fig. 5). The coherence is high

and a phase of about $\pi/2$ dominate for $f < 1$ Hz in the two shoaling wave cases (run 42 and 337). A phase of $\pi/2$ between u and w indicates a dominance of wave orbital motion. For $f > 1$ Hz the co-spectral density and coherence approaches zero, implying that there is no systematic relation between u and w . The spilling wave case (run 98) exhibits a phase of $\pi/2$ for $f < 0.35$ Hz. For $f > 0.35$ Hz u and w are in phase, and the co-spectral density is negative indicating an onshore/downward or offshore/upward fluid motion. This pattern of motion is characteristic for surface-generated turbulence (Ting, 2013). A cut-off frequency of 0.35 Hz in run 98 is, therefore, assumed to result in more robust estimations of turbulent energy.

The shear stress exerted at the seabed by the turbulent motions can be expressed by the Reynolds stress:

$$Re = \rho(u'_v w') \quad (1)$$

(Aagaard and Hughes, 2010) where u'_v is the vector sum of the cross- and longshore turbulent velocities, w' is the vertical turbulent velocity, and ρ is fluid density.

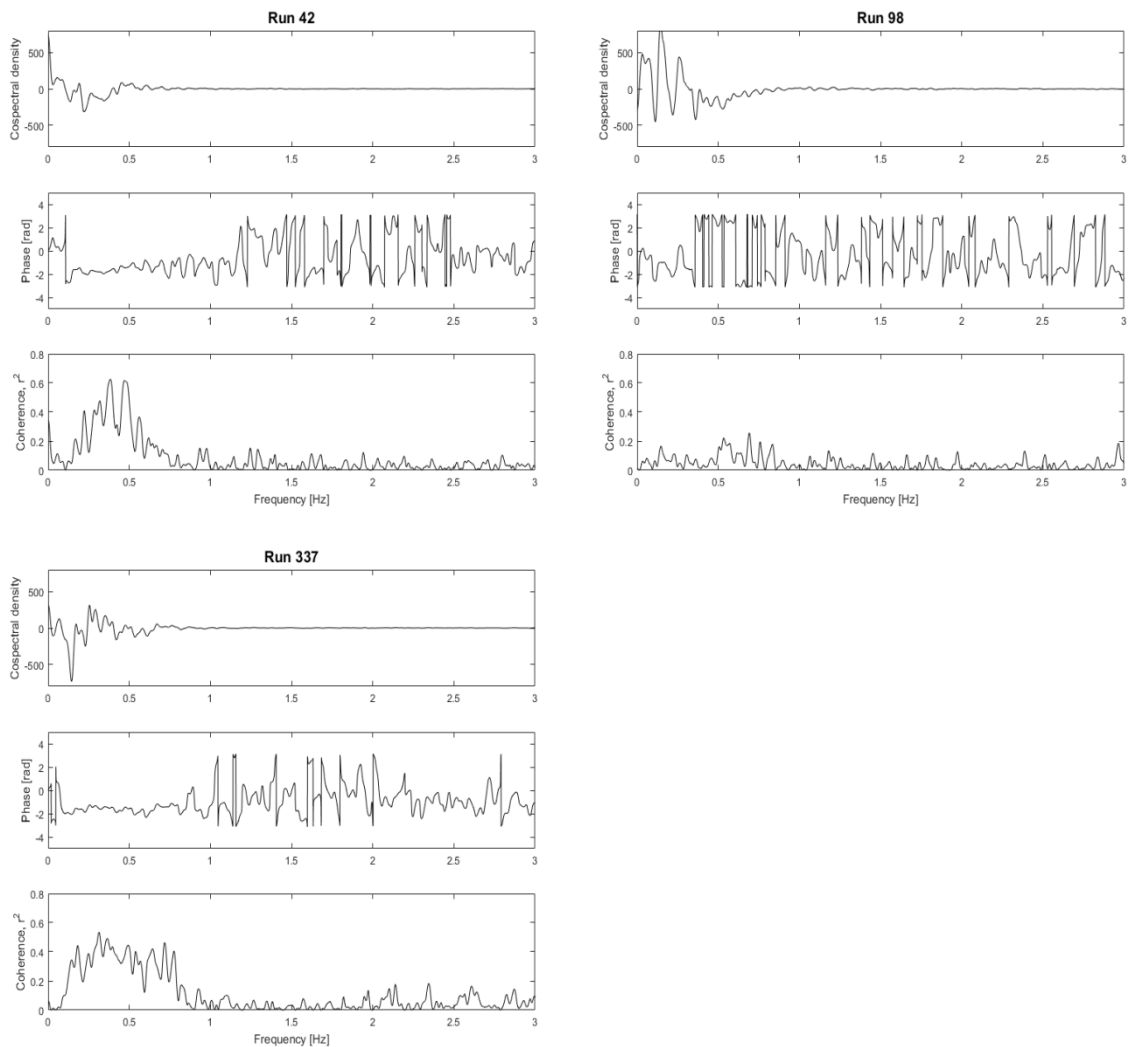


Figure 5. Co-spectral density, phase, and coherence for run 42, 98 and 337

3. Results

The three selected time series are characterized by different hydrodynamic and bedform conditions (Table

1). The two shoaling wave cases are comparable in relation to weak mean currents, small acceleration skewness, and presence of wave ripples. The waves were, however, higher and more velocity skewed during run 337 compared to run 42, and, furthermore, the bedforms were shorter and steeper. According to Wiberg and Harris (1994) the ratio of ripple wavelength to orbital diameter is typically $\lambda/d_0 = 0.65$ for equilibrium vortex ripples. Based on this criteria the bedforms can be classified as vortex ripples during run 42, and as suborbital ripples during run 337 (Table 1).

The spilling wave case (run 98) was more energetic with stronger mean currents, larger acceleration skewness (Table 1), and presence of gently sloping mega ripples (Larsen et al., 2015).

Table 1. Significant wave height (H_s), mean water level (h), cross- and longshore current velocities (U , V), significant horizontal orbital velocity (u_s), orbital diameter (d_0), velocity skewness (SK), acceleration skewness (AS), bed form height (η), spacing (λ), η/λ , and λ/d_0 for run 42, 98 and 337

	Run 42	Run 98	Run 337
H_s [m]	0.42	0.64	0.51
h [m]	1.26	1.61	1.02
U [m/s]	-0.04	-0.15	-0.04
V [m/s]	0.04	-0.42	-0.15
u_s [m/s]	0.62	0.94	0.82
d_0 [m]	1.12	2.06	1.82
SK	0.17	0.58	0.58
AS	0.11	0.27	0.08
η [m]	0.051	0.022	0.046
λ [m]	0.814	2.154	0.460
η/λ	0.06	0.01	0.1
λ/d_0	0.73	1.05	0.25

Short excerpts of the three different time series are presented in Fig. 6. The two shoaling wave cases (run 42 and 337) differentiate with respect to flow velocity and suspended sediment concentration. Flow velocities were highest in run 337, resulting in suspended sediment concentration peaks of nearly two times the magnitude of the peaks in run 42. Moreover, proportionality appears to exist between orbital velocity and suspended sediment concentration in run 337 with peaks in concentration typically beneath the wave crests. This is less evident in run 42. The waves in the spilling wave case (run 98) were less irregular during the one minute excerpt, while distinct peaks in the suspended sediment concentrations were less frequent compared to run 337, and suspended sediment remained in the water column for a longer duration (e.g. $t = 590-610$ s). Furthermore, it appears that the flow was more turbulent (Table 2).

In order to study persistent patterns in the phasing of high suspended sediment concentrations during the wave cycle, and potentially relate the events to the intra-wave variations in turbulence, phase-averages of horizontal orbital velocity (u), suspended sediment concentration (c), Reynolds stress (Re) and wave-induced cross-shore suspended sediment transport rates ($q_x = u \cdot c$) were calculated. The individual waves were identified from zero-up-crossing analyses, and in order to eliminate the influence from high frequency noise or long infra-gravity waves in the records, both a low-pass Hanning filter and high-pass box filter were applied. The cut-off frequencies used were respectively 0.5 Hz and 0.06 Hz.

The phase-averaging was based on 57-95 individual waves containing “coherent events”. “Coherent events” are defined as periods with a suspended sediment concentration higher than the mean concentration plus one time the standard deviation (Jaffe and Sallenger, 1992).

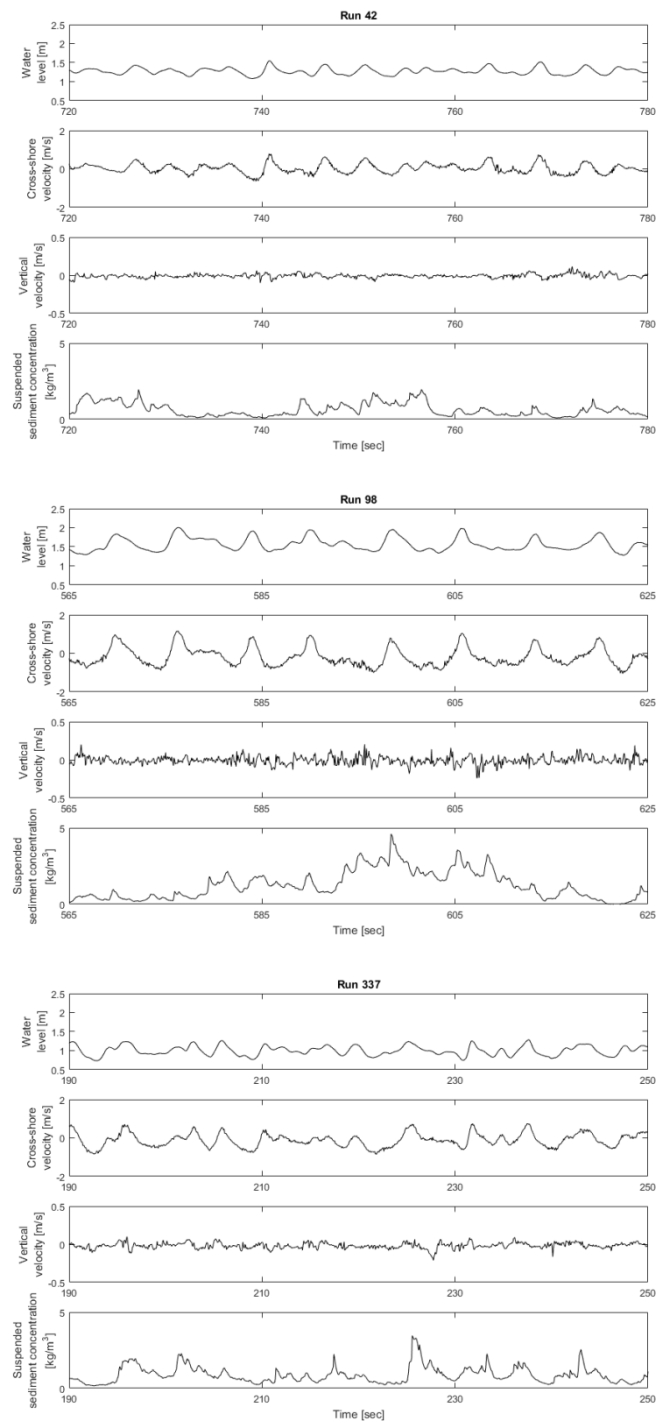


Figure 6. One minute excerpts of time series of water depth (h), cross-shore velocity (u), vertical velocity (w) and suspended sediment concentration (c) during shoaling (run 42 and 337) and spilling wave conditions (run 98)

Table 2. Root mean square (rms) turbulent vertical velocities for run 42, 98 and 337

	Run 42	Run 98	Run 337
w'_{rms}	0.016	0.045	0.021

The resultant phase-averages are presented in Fig. 7. The suspended sediment concentration, normalized with respect to the maximum concentration in the wave cycle (c_{max}) exhibits a distinct phase-dependency in both run 98 and 337, while it is less evident in run 42. In terms of the turbulence (expressed by the Reynolds stress), it was small and highly fluctuating without any significant patterns in the two shoaling cases (run 42 and 337), whereas some consistency in the direction of the turbulent motions appear for the spilling wave case (run 98). Accordingly, it appears that the turbulent motions were consistently upward directed from $t/T = 0.875$ until $t/T = 0.0025$, and followed by downward directed motion from $t/T = 0.0025$ until $t/T = 0.225$.

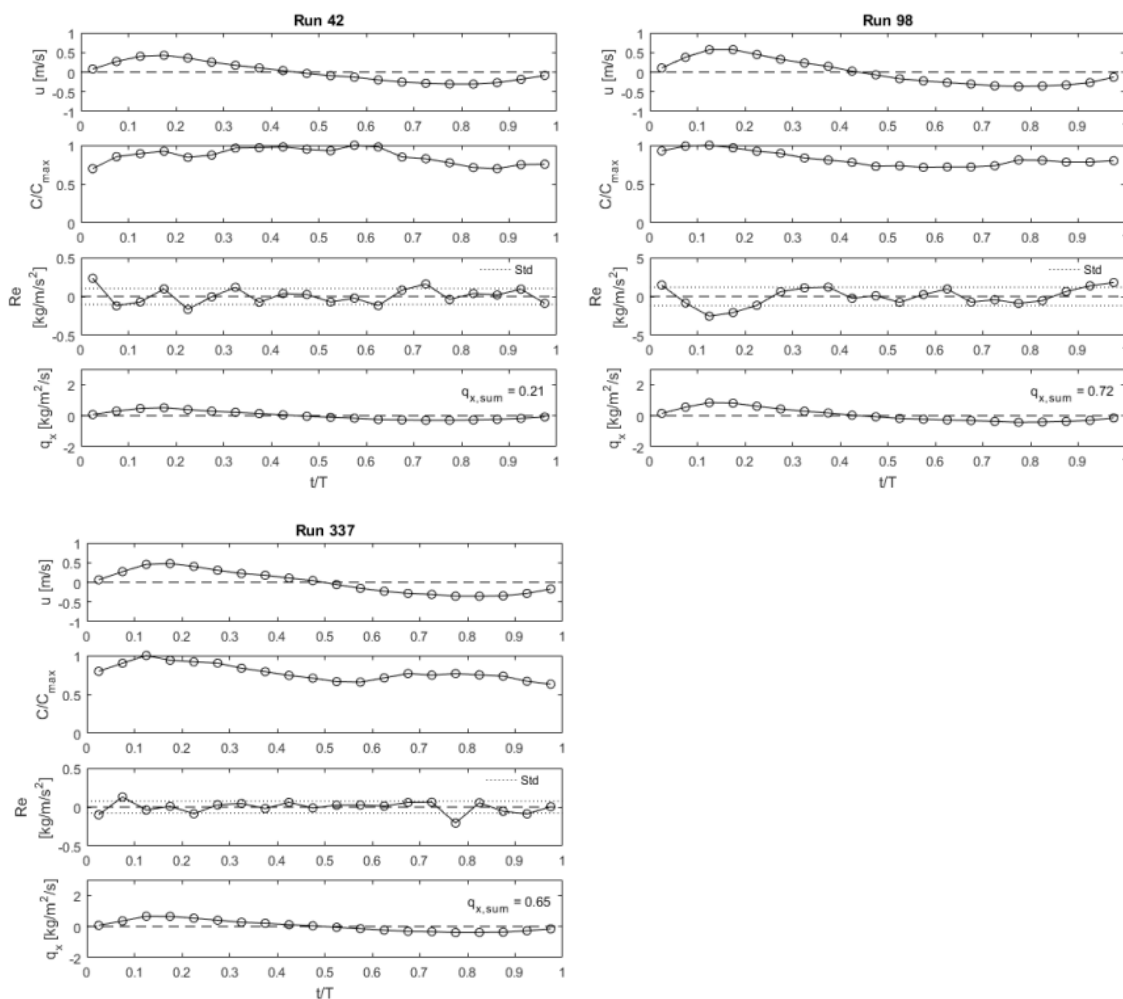


Figure 7. Phase-average plots for run 42, 98 and 337 based on suspension events exceeding a threshold of $\bar{c} + \sigma_c$. Cross-shore wave orbital velocity (u), normalized suspended sediment concentration (C/C_{max}) (normalized with respect to the maximum concentration during the wave cycle), turbulence expressed by the Reynolds stress (Re), and cross-shore wave-induced suspended sediment transport rates (q_x) including the sum over the wave cycle ($q_{x,sum}$). The ADV/OBS were located at respectively $z = 9/10$, $z = 10.5/11.5$ and $z = 9/9$ cm

Run 42 exhibited the highest suspended sediment concentrations around the time of flow reversal (on-off), but trends are not very pronounced. In an attempt to highlight potential patterns, small suspension events, which probably only makes a small contribution to the transport rates, are neglected. An “intense event”-threshold, defined as the mean concentration plus three times the standard deviation (Jaffe and Sallenger, 1992), is therefore applied. This resulted in two distinct peaks in the suspended sediment concentration within the wave cycle about the times of flow reversal with largest concentrations beneath the wave trough (Fig. 8). These intra-wave variations are characteristic in the presence of vortex ripples as sediment laden

vortices will be shed from the bedforms (O'Hara Murray et al., 2011). Accordingly, there is consistency between the observed bedform dimensions (Table 1) and the intra-wave variations of suspended sediment concentration (Fig. 8). The higher suspended sediment concentrations beneath the wave trough than crest are probably a result of the velocity skewness of the waves (Table 1). Nevertheless, the net wave-induced sediment transport rate was onshore directed at the elevation of 10 cm above the bed. It is probably due to the fact that the peak in suspended sediment concentration under the wave trough was very short-lived at $z = 10$ cm, and that the higher velocities under the wave crest were a dominating factor.

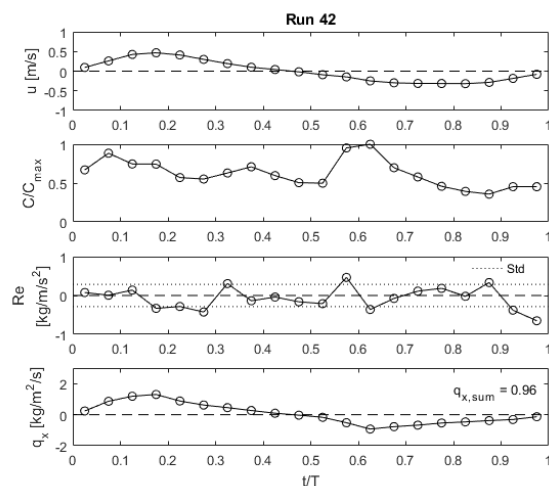


Figure 8. Phase-average plots for run 42 based on suspension events exceeding a threshold of $\bar{c} + 3\sigma_c$. Cross-shore wave orbital velocity (u), normalized suspended sediment concentration (C/C_{\max}) (normalized with respect to the maximum concentration during the wave cycle), turbulence expressed by the Reynolds stress (Re), and cross-shore wave-induced suspended sediment transport rates (q_x) including the sum over the wave cycle ($q_{x,\text{sum}}$). The ADV/OBS were located at $z = 9/10\text{cm}$

The other shoaling wave case, run 337, exhibited different intra-wave variations with peaks in suspended sediment concentration at the time of maximum wave orbital velocity (Fig. 7). This dissimilarity is probably related to the observed change in bedform dimension, which resulted in a smaller ratio of λ/d_0 (Table 1), and, hence, less regular and coherent shedding of vortices (O'Hara Murray et al., 2012). The effect is, therefore, not apparent in the phase-averaged plots. Moreover, breaker-generated turbulence was absent and consequently, the bed shear stress was likely in phase with the orbital motions which, due to the velocity skewness of the waves, caused a net onshore wave-induced sediment transport. Furthermore, significant peaks in Reynolds stress were almost non apparent at the instrument elevation, and this is likely because of the smaller turbulence length scale compared to bedform generated vortices and/or breaker-generated turbulence (Fig. 7).

The spilling wave case (run 98) differed from the shoaling cases by exhibiting higher turbulence levels at $z = 10.5$ cm (Fig. 7 and Table 1) and by containing some phase-consistency. Hence, in contrast to the shoaling cases the sign of the Reynolds stress was not shifting for more or less every measurement. Positive Reynolds stresses, indicating upward directed turbulent motions, appear about the off-to-onshore flow reversal ($t/T = 0.875-0.0025$), followed by downward velocities and negative stresses beneath the wave crest ($t/T = 0.0025-0.225$). This sequence in the main direction of the turbulent motions from up- to downward probably indicates the presence of surface-generated turbulent eddies. Just prior to the wave arrival the water rushes upwards and the low pressure lifts sediment. As the wave breaks, the wave front hits the surface in a motion towards the bed, and finally the eddy motion continues upward. The latter is also weakly indicated in Fig. 7, but the positive peak in the Reynolds stress at $t/T = 0.35$ is not significant.

The duration of this turbulent eddy is related to a period of high suspended sediment concentrations signifying the importance of surface-generated turbulence for sediment suspension. Since the high suspended sediment concentrations occurred on the onshore wave phase, the net wave-induced sediment transport rate was onshore directed.

The bedforms during run 98 were megaripples of low steepness (Table 1). The effect of megaripples to sediment suspension is, for the time being, unknown, and in this case, the surface-generated turbulence seems to have dominated the timing of sediment suspension.

The net wave induced cross-shore suspended sediment transport rates for each of the three examples are presented in Table 3. In all three runs the transport rate was positive indicating a net onshore directed oscillatory transport, but the underlying causes for this, probably differed as implied by the phase-averages (Fig. 7). A small net transport rate (or even negative) might have been expected for run 42 due to the process of vortex shedding beneath the velocity skewed waves. This was, however, not the case, but the transport rate was two to three times smaller than during run 98 and 337.

Table 3. The net wave-induced cross-shore suspended sediment transport rates based on phase-averages over a wave cycle for run 42, 98 and 337

Run	Wave induced cross-shore sediment transport rates [kg/m ² /s] estimated from phase-averages
42	0.021
98	0.072
337	0.065

4. Discussion and conclusions

In this study three examples of intra-wave variations in suspended sediment concentration during different hydrodynamic and bedform conditions were presented. Phase-averaging was applied to waves containing suspended sediment concentration above a threshold of $\bar{c} + \sigma_c$ in order to study persistent patterns in the timing of high suspended sediment concentration during a wave cycle. By neglecting small, inconsistent suspension events the intra-wave variations in suspended sediment concentration become more distinct, and it facilitates the data interpretation. Accordingly, it is an underlying assumption that the small suspension events make negligible contribution to the transport rates. This is supported by several studies e.g. Cox and Kobayashi (2000), Ruessink (2010), and Yoon and Cox (2012). In the latter, it was, for instance, determined that “coherent events” (> mean + std.) of respectively suspended sediment concentration and turbulence occurred in less than 10 % of the time series but contained about 40-45 % of respectively the sediment and fluid motion.

The phase-averaged plots for the spilling wave case (run 98) indicated the existence of surface-generated turbulent eddies on the onshore wave phase at $z = 10.5$ cm, concurrent with high suspended sediment concentrations. This is contrary to the findings of earlier laboratory studies. According to Nadaoka et al. (1989) the turbulence generated by spilling breakers develops into obliquely descending eddies which approach the bed with a considerable time-lag compared to the time of breaking. Therefore, large near-bed turbulence is often observed during the offshore wave phase for spilling breakers at least in laboratory experiments. For instance, co-occurrence of high concentration events and turbulent events took place during the offshore wave phase for about 60-70 % of the time in the study by Scott et al. (2009).

Beneath shoaling waves (run 42 and 337) the turbulent velocities were small at about $z = 10$ cm (Fig. 7). This is consistent with Scott et al. (2005) who reported that surface-generated turbulence beneath shoaling waves was almost non-existing. The bed morphology is therefore relatively more important for sediment suspension in these cases. The presence of vortex ripples in run 42 highly affected the proportionality between the orbital velocity and suspended sediment concentration. This is comparable with the findings of previous laboratory measurements (e.g. O’Hara Murray et al., 2011).

The considerable effect of both surface-generated turbulence and bedform dimensions for the timing of high suspended sediment concentrations within the wave cycle emphasises the need of including these parameters in sediment transport models in order to make accurate estimates of the net suspended sediment transport direction during low-moderate energy conditions.

References

- Aagaard, T. and Hughes, M.G., 2006. Sediment suspension and turbulence in the swash zone of dissipative beaches. *Marine Geology*, 228: 117-135.
- Aagaard, T., and Hughes, M.G., 2010. Breaker vortices and sediment suspension in the surf zone. *Marine Geology*, 271: 250-259.
- Bagnold, R.A., 1966. An approach to the sediment transport problem from general physics. *Geological Survey Professional Paper*, 422-I, US Government Printing Office, Washington.
- Cox, D.T. and Kobayashi, N., 2000. Identification of intense coherent motions under shoaling and breaking waves. *Journal of Geophysical Research*, 105: 14223-14236.
- Elgar, S., Gallagher, E.L. and Guza, R.T., 2001. Nearshore sandbar migration. *Journal of Geophysical Research*, 106: 11623-11627.
- Grasso, F., Castelle, B. and Ruessink, B.G., 2012. Turbulence dissipation under breaking waves and bores in a natural surf zone. *Continental Shelf Research*, 43: 133-141.
- Hay, A.E., 2011. Geometric bed roughness and the bed state storm cycle. *Journal of Geophysical Research*, 116, C04017.
- Jaffe, B. and Sallenger, A., 1992. The contribution of suspension events to sediment transport in the surf zone. *Proceedings of 23rd Conference on Coastal Engineering*, Venice, Italy, chapter 205.
- Larsen, S.M., Greenwood, B. and Aagaard, T., 2015. Observations of megaripples in the surf zone. *Marine Geology*, 364: 1-11.
- Marino-Tapia, I.J., O'Hare, T.J., Russell, P.E., Davidson, M.A. and Huntley, D.A., 2007. Cross-shore sediment transport on natural beaches and its relation to sandbar migration patterns: 2. Application of the field transport parameterization. *Journal of Geophysical Research*, 112, C03002.
- Nadaoka, K., Hino, M. and Koyano, Y., 1989. Structure of the turbulent flow field under breaking waves in the surf zone. *Journal of Fluid Mechanics*, 204: 359-387.
- Nielsen, P., 2006. Sheet flow sediment transport under waves with acceleration skewness and boundary layer streaming. *Coastal Engineering*, 53: 749-758.
- O'Hara Murray, R.B., Thorne, P.D. and Hodgson, D.M., 2011. Intrawave observations of sediment entrainment processes above sand ripples under irregular waves. *Journal of Geophysical Research*, 116, C01001.
- O'Hara Murray, Hodgson, D.M. and Thorne, P.D., 2012. Wave groups and sediment resuspension processes over evolving sandy bedforms. *Continental Shelf Research*, 46: 16-30.
- Puleo, J.A., Holland, K.T., Plant, N.G., Slinn D.N. and Hanes, D.M., 2003. Fluid acceleration effects on suspended sediment transport in the swash zone. *Journal of Geophysical Research*, 108, C11.
- Ruessink, B.G., 2010. Observation of Turbulence within a Natural Surf Zone. *Journal of Physical Oceanography*, 40: 2696-2712.
- Scott, C.P., Cox, D.T., Maddux, T.B. and Long, J.W., 2005. Large-scale laboratory observations of turbulence on a fixed barred beach. *Measurement Science and Technology*, 16: 1903-1912.
- Scott, N.V., Hsu, T.-J. and Cox, D., 2009. Steep wave, turbulence, and sediment concentration statistics beneath a breaking wave field and their implications for sediment transport. *Continental Shelf Research*, 29: 2303-2317.
- Seuront, L., Yamazaki, H. and Schmitt, F.G., 2005. Intermittency, in: Baumert, H.Z., Simpson, J.H. and Sündermann, J. (ed.): *Marine Turbulence – Theories, Observations, and Models*, Cambridge University Press, 66-78.
- Smyth, C., Hay, A.E. and Zedel, L., 2002. Coherent Doppler Profiler measurements of near-bed suspended sediment fluxes and the influence of bed forms. *Journal of Geophysical Research*, 107: 10.1029.
- Ting, F.C.K., 2013. Laboratory measurements of large-scale near-bed turbulent flow structures under plunging regular waves. *Coastal Engineering*, 77: 120-139.
- Wiberg, P.L. and Harris, C.K., 1994. Ripple geometry in wave-dominated environment. *Journal of Geophysical Research*, 99: 775-789.
- Yoon, H.-D. and Cox, D.T., 2012. Cross-shore variation of intermittent sediment suspension and turbulence induced by depth-limited wave breaking. *Continental Shelf Research*, 47: 93-106.